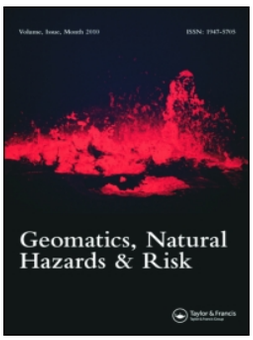

Geomatics, Natural Hazards and Risk

ISSN: 1947-5705 (Print) 1947-5713 (Online) Journal homepage: https://www.tandfonline.com/loi/tgnh20

Monitoring the deformation and strain analysis on the Ataturk Dam, Turkey

H. H. Yavaşoğlu, Y. Kalkan, İ. Tiryakioğlu, C .O. Yigit, V. Özbey, M. N. Alkan, S. Bilgi & R. M. Alkan

To cite this article: H. H. Yavaşoğlu, Y. Kalkan, İ. Tiryakioğlu, C .O. Yigit, V. Özbey, M. N. Alkan, S. Bilgi & R. M. Alkan (2018) Monitoring the deformation and strain analysis on the Ataturk Dam, Turkey, Geomatics, Natural Hazards and Risk, 9:1, 94-107, DOI: 10.1080/19475705.2017.1411400

To link to this article: https://doi.org/10.1080/19475705.2017.1411400

Published online: 12 Dec 2017.

GEOMATICS, NATURAL HAZARDS AND RISK, 2018
VOL. 9, NO. 1, 94–107
https://doi.org/10.1080/19475705.2017.1411400

Taylor & Francis
Taylor & Francis Group

Monitoring the deformation and strain analysis on the Ataturk Dam, Turkey

H. H. Yavaşoğlu[a], Y. Kalkan[a], İ. Tiryakioğlu[b], C .O. Yigit [c], V. Özbey[a], M. N. Alkan[d], S. Bilgi[a] and R. M. Alkan[a,d]

[a]Department of Geomatics Engineering, Faculty of Civil Engineering, Istanbul Technical University, Istanbul, Turkey; [b]Department of Geomatics Engineering, Faculty of Engineering, Afyon Kocatepe University, Afyon, Turkey; [c]Department of Geomatics Engineering, Faculty of Engineering, Gebze Technical University, Turkey; [d]Hitit University, Corum, Turkey

ABSTRACT

Every man-made structure creates certain risks — dams are no exception. Most failures in man-made structures that have occurred could have been avoided if the structures' behaviour had been inspected, monitored, and analyzed continuously, and if proper corrective measures had been taken in a timely fashion. The DSI (The General Directorate of State Hydraulic Works), which is the institution responsible for dam safety, has long used surveying methods to measure the displacements of geodetic points as a part of dam monitoring policy. In this study, we focus on the dam's mechanical behaviour throughout a time period of more than 10 years. These study results have been derived from a separate, ongoing project that has monitored deformation on the Ataturk Dam and is now determining the water level of the reservoir. The project results show that although the dam body has become more stable and the water load behind the dam has increased, the rate of displacement of the dam has declined significantly. From these results, it can be seen that the reservoir water level can be increased evenly over time and that 542 m is the maximum water level of the dam's reservoir.

ARTICLE HISTORY
Received 5 July 2017
Accepted 6 November 2017

KEYWORDS
Ataturk Dam; deformation; GNSS; terrestrial measurements

1. Introduction

Structures such as dams are important for water supply, flood control, agriculture, and hydroelectric power production. Numerous dams are constructed worldwide for these purposes. With the development of construction technology, especially in the 1970 s, dams with huge capacities have been built. By the year 2000, there were 45.000 grand dams and 800.000 small dams constructed globally (Ponseti and López-Pujol 2006). Dams with crest heights taller than 300 m and reservoirs above 200 million m^3 have been constructed in the last century. The dam with the highest crest (335 m) is the Rogun Dam in Tajikistan (Singh 2013). Of these dams, the one with the largest capacity, The Synrude Tailings Dam, was built in Canada with a 5.40 billion m^3 reservoir capacity. But after that, a new dam was constructed in China, the Three Gorges Dam; it has the largest reservoir, with 39.3 billion m^3 greater than the Synrude Tailings Dam, and 22.500 MWs of hydroelectric power production capacity (Behr et al. 1998; Li and Wang 2011; Boulanger and Montgomery 2016).

These structures have certain risks, just like other man-made structures. Hazard assessment of the increasingly aging dams is mandatory, yet complex procedure. There are some challenges with

CONTACT Y. Kalkan kalkany@itu.edu.tr

these evaluations, especially if the original installation, design, and construction details are unknown or not defined clearly. A safety assessment of the dams involves filed surveillance, periodic safety observations, operation procedure tests, scheduled maintenance, and preparation for emergency situations. Risk-based dam safety procedures include traditional safety management applications with the integration of recognition on analysis of risks, and formal assessment of the uncertainties. Dam safety analysis relies on having a philosophy that is able to represent a wide range of risks and uncertainties in a practical way. This includes the engineering and scientific characterization of these parameters by using available techniques and monitoring physical performance in their natural environment. Such physical data present the most important issues while evaluating the safety and performance of both concrete and embankment formation dams (Liu et al. 2016). These issues are movement, water pressure, seepage, reservoir and tail water elevations, local seismic activity, total pressure, stress, strain, internal concrete and environmental temperature, and precipitation (Jansen 1983; ICOLD 1992). These physical data are measured and monitored frequently to acquire information necessary for analyzing and defining a problem. For example, the downstream movement of a dam due to high reservoir water pressure must be analyzed to determine whether the movement is distributed uniformly along or in the dam, the foundation, or both, and to assess whether the movement is increasing, decreasing, or stable. Such information can be used to determine proper corrective measurements (Manake and Kulkarni 2002; Chen et al. 2016; Kan and Taiebat 2016).

Ataturk Dam is 169 m in height and has a total volume of 84.500 hm^3, whereas the reservoir's volume is 48.700 hm^3 and area is 817 km^2. The approximately 900.000 km^2 area in Harran Plain, Sanliurfa is irrigated by the water provided by the dam using tunnels and pipe stations. Moreover, the drinking and usable water of Şanlıurfa is obtained from the Ataturk Dam. The dam also feeds a hydroelectric power plant which provides a significant amount of energy to Turkey. The capacity of the dam is 2.400 MW with 8.9 billion KWh of annual power production. Ataturk Dam in the northwest of Şanlıurfa, which is the biggest dam in Turkey and 11th worldwide according to its capacity, was evaluated with data derived with various techniques since 2006. Evaluation of the velocity and strain field of the dam is discussed and presented in this paper.

2. Deformation monitoring on dams

The monitoring of dam performance is a critical element in producing and maintaining a safe dam. Monitoring programmes typically consist of surveillance or visual observation, instrumentation, data collection, data evaluation, analysis, management, and decisions/response based on results (FEMA 2015). Surveillance and monitoring programmes on dams provide information for evaluating the dam's performance with respect to intention of design and expected behaviour. Monitoring the changes could affect the safety performance assessment of a dam, can assist the investigations and evaluations of abnormal dam performance, and determine if maintenance is necessary. Dams and their surrounding areas can be monitored with a variety of techniques to find out if horizontal and/or vertical deformations will arise in time. Because these data focus on particular areas of the dam that have moved, inspectors are alerted to look for potential problems during the visual inspection. Movement can cause damage or structural distress in concrete dams, and cracking and sliding in embankment ones. Dams and their environments should be monitored on a regular basis by available methods, which include geodetic and non-geodetic measurements. Non-geodetic survey devices consist of settlement sensors, inclinometers, extensometers, tiltmeters, plumblines, crack and joint measuring devices, stress-strain-joint and internal temperature meters in the baseplate of the embankment, and crossarms on the structure. Generally, movement and/or deformation of the structure are monitored and can be detected by geodetic methods. The type of dam and the predictive deformation are taken into consideration when determining the type of surveillance, time period of the surveillance, and related standards.

3. Deformation monitoring of Ataturk Dam by using geodetic methods

Geodetic methods for monitoring dam deformations range from terrestrial/conventional observations to space-based measurements like GNSS and interferometry. Different equipment and devices have been used based on the geodetic methods, such as theodolites for alignment measurements, total stations for conventional location measurements, levels for levelling surveys, GNSS receivers for space-based measurements, and SAR images for interferometric applications (Manake and Kulkarni 2002; USACE 2002; Tasci 2008; Kalkan et al. 2010; Yigit et al. 2016).

In this study, deformation monitoring of the Ataturk Dam has been performed periodically to determine the horizontal displacements using conventional (terrestrial) measurements from 2006 to 2013 and satellite-based (GNSS) techniques from 2007 to 2013 (11 periods for Terrestrial Measurements & 9 periods for GNSS, Table 1). The 25 reference stations outside the deformation zone have been established, and deformations on the dam embankment and the surrounding area have been evaluated with respect to these points. Potential deformation zones are represented with 217 object points (deformation points) (Figure 1(a,b)).

3.1. Terrestrial measurements

Terrestrial measurements may include conventional geodetic measurements which involve distance, horizontal, and vertical angle observations by optical/electronic total station instruments (Lambeck 1979). In this study, angle and distance measurements were performed with the TDA 5005 Total Station, the Wild T3000 electronic Theodolite, and the Distomat DI3000.

Although there were 25 reference stations, angles and distance measurements were carried out with conventional terrestrial methods on 13 of the stations closer to the dam in the study. Angles were measured with three complete sets, and distances were obtained conjugately. Two hundred and seventeen object points' coordinates were calculated from 13 reference stations to establish correlation between them. Angles to the object points were observed within the two faces of the instruments.

Table 1. The time schedule of the measurements (GNSS-▲ and Terrestrial-X).

	2006	2007	2008	2009	2010	2011	2012	2013
May	X	X-▲	X-▲					
November	X	X-▲	X-▲	X-▲	X-▲	X-▲	X-▲	X-▲

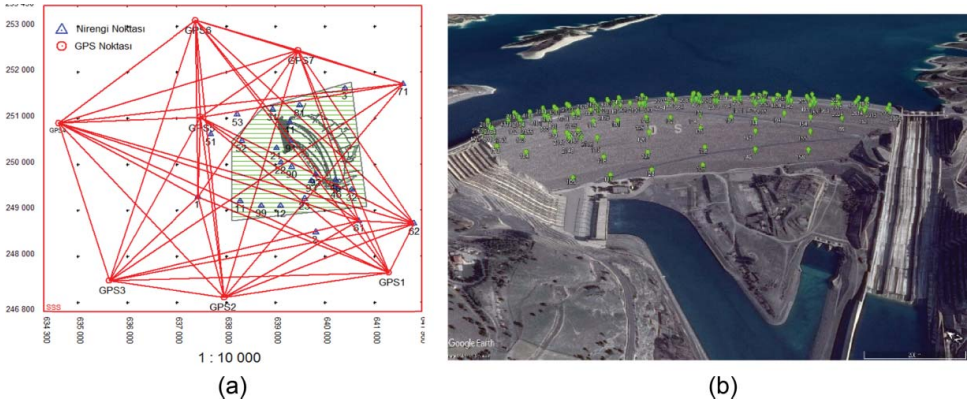

Figure 1. **(a).** Reference network/stations. **(b).** Object (deformation) network/points.

Table 2. GNSS Equipment.

Instrument	Number	Firm
Geodetic GNSS Rec	4	Topcon Hiper GGD&PLUS
Geodetic GNSS Rec	3	Sokkia GRX1
Geodetic GNSS Rec	3	Ashtech Z-Xtreme with Geodetic Antenna IV
Geodetic GNSS Rec	3	Thales Z-Max and Antenna

3.2. GNSS measurements

GNSS is a powerful technique to determine deformation on engineering structures, e.g. dams and bridges. GNSS has become more common due to its accuracy and cost-effective structure, making it preferable to classical surveying techniques in deformation analysis. Receivers that can record GNSS data were used in this project (Table 2).

GNSS observations on the 25 reference stations were conducted with at least 10 h of observations, 5-s data interval, and 10° of elevation mask. On the other hand, object points were measured based on at least 5 reference stations for 40 min long with the same properties of data interval and elevation mask (Figure 2).

Reference stations using both terrestrial measurements and GNSS survey are constructed as pillars with a force-centred design to eliminate blunder errors. The force-centred components were used to fix the GNSS antenna on object points (Figure 3).

To process the GNSS data, Leica Geo Office software was used with the IGS final satellite orbit information. In the first step, the raw data were converted to RINEX format and the final orbits were downloaded. In the next step, reference stations were processed internally. After obtaining the control of the reference stations when they have no deformation between two periods, the object points were evaluated with respect to these reference stations. Finally, the results were transformed according to the first epoch of observations.

4. Conventional deformation analysis

Conventional deformation analysis (CDA) method in a geodetic network is explained in detail by Hekimoglu et al. (2010); it is based on the difference in coordinates between two observation epochs.

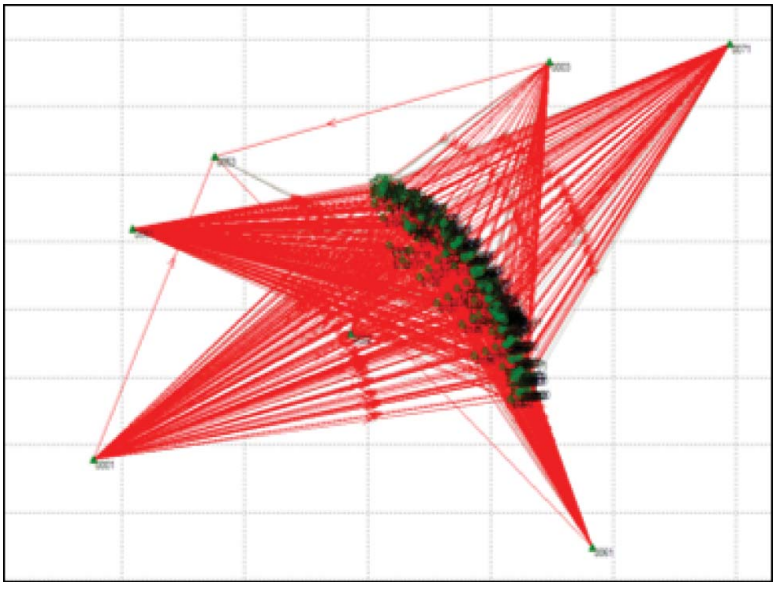

Figure 2. GNSS network reference stations and object points.

Figure.3. Pictured at the top are the reference stations with GNSS equipment. Below them is the object point with a target for angle measurement.

These differences, called 'displacements,' occur when the expected movements are rejected by statistical tests. The reference network in this study is adjusted as a free network for each epoch.

The Gauss–Markov model is simply explained as follows:

$$\begin{aligned} l_1 \; + \; v_1 &= \mathbf{A}_1 x_1 \;\; C_{l_1 l_1} = \sigma_0^2 \, \mathbf{P}_1^{-1} \\ l_i \; + \; v_i \; &= \mathbf{A}_i x_i \;\; C_{l_i l_i} = \sigma_0^2 \, \mathbf{P}_i^{-1} \end{aligned} \tag{1a}$$

and

$$\begin{aligned} x_1 &= \left(A_1^T P_1 A_1\right) + A_1^T P_1 l_1 \\ x_i &= \left(A_{(i)}^T P_i A_i\right) + A_{(i)}^T P_i l_i \end{aligned} \tag{1b}$$

where the subindices are, 1 = first epoch, i = second (last) epoch, $\mathbf{A}$ = design matrices, $\boldsymbol{x}$ = vector of estimated coordinate, $\mathbf{P}$ = the weight matrix, $\boldsymbol{l}$ = observation vector, and $\boldsymbol{v}$ = residual vector.

In the application of CDA, a global congruency test is implemented to evaluate if there is any significant displacement between two epochs. According to the model, if the coordinates of the corresponding points between two epochs changed according to expectations, they form the null hypothesis.

Hypothesis

$$H_0 : \ E\ (x_1) = E\ (x_i) \tag{1c}$$

and is tested against its alternative

$$H_0 : E\ (x_1) \neq E\ (x_i) \tag{1d}$$

where E stands for 'expectation.'

It is clear that the datum between two epochs must be the same. It is managed by taking the approximate coordinates of the identical stations as the same in both epochs. The adjustment of each epoch is carried out as a free network and the points' coordinates (assumed identical) are determined as unknown. Then, the influence of the null hypothesis on the least squares estimation (LSE), in the absence of correlations between epochs, results in (Pelzer 1971; Koch 1985; Niemeier 1985; Pelzer 1985; Cooper 1987)

$$R = d^{\mathrm{T}} \mathrm{Q}_{\mathrm{dd}}^{+} d \tag{2}$$

$$d = xi - x1 \tag{3}$$

$$Q_{\mathrm{dd}} = \ Q_{x1x1} + \ Q_{xixi} \tag{4}$$

$$s_0^2 = \frac{v_1^{\mathrm{T}} P_1 v_1 + v_i^{\mathrm{T}} P_i v_i}{f1 + f\mathrm{i}} \tag{5}$$

$$T = \frac{R}{h s_0^2} \ \sim F_{h,f,\alpha} \tag{6}$$

under the assumption of normally distributed observation errors. In the equations above, Q_{x1x1} and Q_{x2x2} = cofactor matrices; $f = f_1 + f_i$ = sum of the degrees of freedom at either epoch; $\boldsymbol{d}$ = differential vector of estimated coordinates; Q_{dd} = cofactor matrix of $\mathbf{d}$ and Q_{dd} + its pseudo inverse; h is the rank of the matrix Q_{dd}; and α = chosen error probability. Here, s_0^2 denotes the estimated variance component in the absence of the null hypothesis. If $T > F_{h,f,\boldsymbol{\alpha}}$, then the null hypothesis is rejected.

Therefore, the result of an unexpected displacement is obtained from the difference in the coordinates between two epochs. After that, its localization is carried out. There are numerous localization methods for deformation analysis in the literature. In this study, the S-transformation method was used (Baarda 1973; Niemeier 1985; Cooper 1987; Welsch et al. 2000).

After the adjustment and estimation for each epoch, the results were compared with sequential couple-epochs to decide if these epochs should be combined. The double period analysis is implemented with a stochastic test for each period.

The test value (f) in the Fisher distribution is defined as

$$fr \ = \ m_1^2 / \ m_i^2 \tag{7}$$

where m_1^2 and m_i^2 are mean-square-error values of unit measure for the first and last (ith) period, respectively. The test value for Equation 7 was calculated with a 0.05 margin of error. Table values F (f_1; f_i), where f_1 and f_i denote degree of freedom for the first and last period observations, respectively, were compared to see if the condition ($f_L < F_L$) for the levelling results was met. When the levelling condition was procured, the displacement vectors were determined by Equation 3, and their test criteria were calculated according to the rule

$$\begin{aligned} &dX_i = \ X_i - \ X_1; \quad dY_i = \ Y_i - \ Y_1; \quad dP_i = \left(dX_i^2 + \ dY_i^2\right)^{1/2} \\ &m_i = \ \left(m_{xi}^2 + \ m_{yi}^2\right)^{1/2} \qquad\qquad (i = 1 \ , \ \text{first period} \ ; \ i = \ \text{last period} \ (i > 1)) \\ &M_i = \left(m_1^2 + \ m_i^2\right)^{1/2} \end{aligned} \tag{8}$$

and their test criteria were calculated according to the rule test value (Hoover and Rockville 1984),

$$T_i = 2,5*(\ M_i)\sqrt{a^2 + b^2}. \tag{9}$$

We used the test values computed from Equation 9 to calculate the significant displacement (dPi > Ti).

Eleven epochs of conventional terrestrial geodetic observations and nine epochs for GNSS observations were carried out through 2006–2013. The same equipment and hardware were used through similar observation methods. First, double period analysis was used to find out whether stations on the reference network had moved or not. Then, observations on the object points based on the reference stations, which were accepted to have no movement, were adjusted, and double period analysis was implemented based on the results. Displacement vectors for the compared periods and their accuracy criteria were calculated according to the given formula (8). Calculated displacement was tested with the formula (9) to find out whether there was significant movement, and 90% of the object points were defined to have meaningful horizontal movement. These movement vectors' perpendicular components to the crest axis (radial displacement vector) are about 84% meaningful. The displacement vectors for the 30 object points having maximum deformation on the dam body are given in Figure 4 and Table 3, and all displacement vectors are shown in Figure 5.

5. Strain analysis of dam

Strain is strictly related to displacement and is the displacement with the adjacent points in physical and mechanical bonds. Displacement can be considered as the difference in the Cartesian Coordinates of the same point at different times. The correlation between coordinates of a point at time t1 and time t2 under homogenous deformation can be explained with a simple affine transformation (Brunner 1979).

With this approach, variance for the relative location can be obtained by (Kakkuri and Chen 1992)

$$du = (E + \mathbf{w})r + t_0 \tag{10}$$

Figure 4. Location of the 30 object points having maximum displacement vectors.

Table 3. Results of the deformation analysis (displacement values) obtained from GNSS and terrestrial measurements.

Period of the measurements			2007–2013	2007–2013	2006–2013	2007–2013
Point ID	Longitude (°)	Latitude (°)	GNSS dPi (cm)	Terrestrial dPi (cm)	Terrestrial dPi (cm)	GNSS–Terrestr Diff. (cm)
2082	38.3208	37.4823	18.1	16.9	21.1	1.2
2112	38.3186	37.4844	16.7	16.6	20.8	0
4050	38.3209	37.4821	16.3	17.3	20.8	−1
2111	38.3187	37.4845	14.9	15.9	19.4	−0.9
2062	38.3219	37.4808	14.9	16.1	19.3	−1.2
2102	38.3194	37.4838	15.6	15.3	18.9	0.3
2092	38.3201	37.483	15.4	14.9	18.4	0.6
2101	38.3194	37.4838	14.9	14.3	18.2	0.6
2042	38.3229	37.4791	13.5	14.8	17.7	−1.3
2103	38.3192	37.4836	12.6	13.2	16.7	−0.6
2061	38.3222	37.4809	11.8	13.6	16.6	−1.8
2072	38.3214	37.4816	13.9	13.5	16.5	0.4
2091	38.3202	37.4831	14.1	13.4	16.5	0.7
2100	38.3195	37.4839	12.4	12.8	16.4	−0.4
2122	38.3177	37.485	13.5	13.1	16.4	0.4
4010	38.3232	37.4785	11.7	14.1	15.9	−2.4
2081	38.3209	37.4823	13.1	13.1	15.7	0
2058	38.3222	37.48	11.2	12.4	15.3	−1.2
4020	38.3227	37.4795	10.5	12.7	15.1	−2.2
974	38.3205	37.482	11.8	11.1	15	0.7
2121	38.3178	37.4851	12	11.6	15	0.4
2094	38.3197	37.4828	10.5	11.8	14.8	−1.3
2076	38.3205	37.4819	10.3	11.7	14.7	−1.4
2104	38.3192	37.4836	10.2	11.9	14.6	−1.6
994	38.3214	37.4808	11.2	11	14.5	0.2
2063	38.3217	37.4807	10.4	10.8	14.4	−0.4
984	38.3209	37.4814	10.4	10.7	14.1	−0.3
2071	38.3216	37.4816	11.5	10.9	13.9	0.6
2057	38.3223	37.4801	10.5	10.4	13.5	0.1
2120	38.3178	37.4852	10.6	10.7	12.6	−0.1

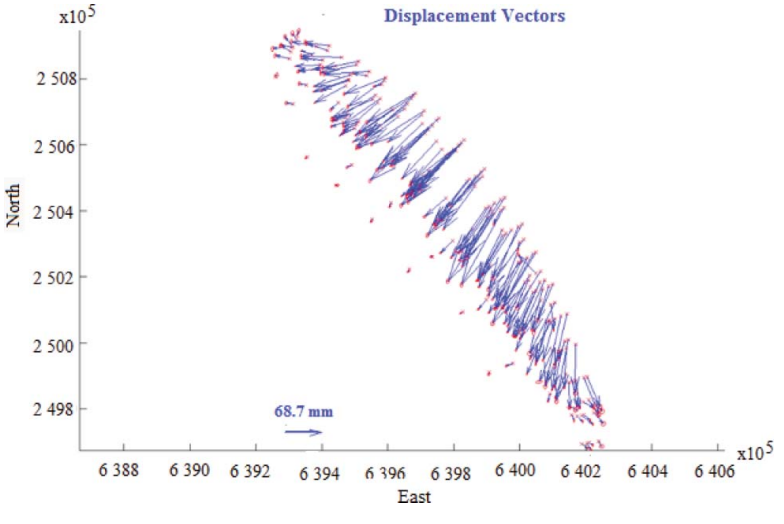

Figure 5. The dam horizontal displacement.

where E is the symmetric strain tensor, $\mathbf{w}$ is the inverse symmetric strain tensor, t_0 is the translation solid block movement for all the points, and r is the coordinate. Also, translation can be explained by

$$t_0 = [t_1 t_2]^T \tag{11}$$

$$d_u^T = [u_x \quad u_y],\ r = [x\ y]^T \tag{12}$$

Symmetric strain tensor is obtained by

$$E = \begin{bmatrix} \varepsilon_{xx} & \varepsilon_{xy} \\ \varepsilon_{yx} & \varepsilon_{yy} \end{bmatrix} \tag{13}$$

Diagonal elements of the symmetric tensor define the dilation along the coordinate axes, and other elements off the diagonals define the small, angular disturbances through deformation according to the coordinate axes. (Doğan 2017). The inverse symmetric tensor is the differential rotation of the solid block due to deformation for the plane including coordinate axes.

$$w = \begin{bmatrix} 0 & w \\ -w & 0 \end{bmatrix} \tag{14}$$

If d_u deformation vector is the result of the affine transformation within the epochs t_1 and t_2, it can be calculated as (Brunner 1979)

$$d_u = Bu \tag{15}$$

The matrix of the coefficients B is shown as

$$B = \begin{bmatrix} x & y & 0 & y & 1 & 0 \\ 0 & x & y & -x & 0 & 1 \end{bmatrix} \tag{16}$$

If the Equations (14) and (15) readjusted according to (12) and (13) and were written in the Equation (16) (Prescott 1976; Brunner 1979; Lambeck 1988; Deniz 1990; Doğan 2017)

$$\begin{bmatrix} u_x \\ u_y \end{bmatrix} = \begin{bmatrix} x & y & 0 & y & 1 & 0 \\ 0 & x & y & -x & 0 & 1 \end{bmatrix} \begin{bmatrix} \varepsilon_{xx} \\ \varepsilon_{xy} \\ \varepsilon_{yy} \\ w \\ t_1 \\ t_2 \end{bmatrix} \tag{17}$$

Strain parameters are obtained by the least squares method. To calculate the strain analysis, the velocity field of the deformation area on the dam was derived from GNSS data (Table 3). As given in Table 3, the results of the deformation analysis obtained from both GNSS and terrestrial measurements are very coherent. Differences between the two methods range from −2.4 cm to 1.2 cm.

The strain analysis of the dam that was conducted by using its velocity field was processed by Grid Strain Matlab Toolbox. The software can calculate the deformation (rate) field for an area using displacements/velocities of points covering the whole study area. Grid strain provides the intensity and direction of the principal components of strain tensor in each point of the grid, as well as the

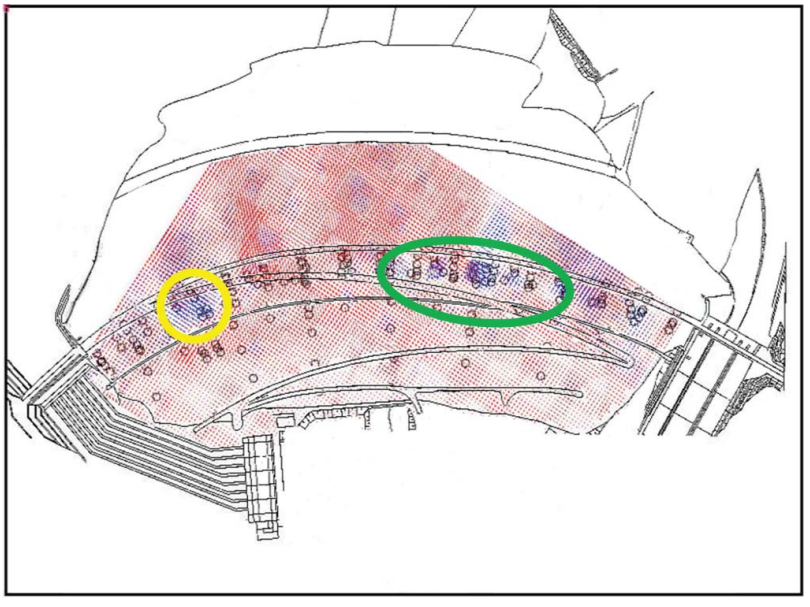

Figure 6. Strain analysis of the dam, ellipse and circle are explained in text.

significance of the results obtained on the basis of spatial distribution and accuracy of available measurements (Pesci and Teza 2006; Gülal 2013).

After the process, the obtained results (the strain field tensors [consisting of the principal strain directions, Eigen vectors, and the Eigen values in each computation point], change in the area like the strain tensor trace, the prevalent Eigen value, and shear normalized strain trace) are shown as contours (Teza et al. 2008). The software automatically computes the grid length based on station baselines, generally on the spacing of the experimental points. The standard deviation of all the inner distances between the pairs of points were computed and assumed as the default values. The programme automatically defines the smoothing parameter, or scale factor, for the modification of the least square weighting matrix as given in Zhu-Jiang and Gang (1996). All the available data are involved in computation, but errors are rescaled using an appropriate function, which increases with distance. The detailed explanation of this programme is available in Pesci and Teza (2006) and Gülal (2013).

2D strain analysis was executed in this study. The study area was divided into 10 × 10 m grids, and strain fields for the corners of the grids were calculated. The arrows in Figure 5 show the temporal displacement vectors. Grid strain software calculates the amount of deformation between GNSS points iteratively. Data density and magnitude of the deformation can affect the displacement vectors given in Figure 5.

Maximum water pressure generally occurs in the middle of the dam body. Pressure in the middle is transferred to the edges with the help belt construction. When examining Figure 6, it can be seen that the maximum strains are in the middle and right-middle points. Vertical regimes are active, especially with the water pressure in these regions. This result is compatible with deformation analyses. Also according to Figure 6, the right-middle part of the dam body (ellipse) and the old stream bed have the largest deformation. Additionally, there is another zone to the left of the body (circle) where deformation occurred. These two zones are the regions where the most movement was observed after the construction of the dam, so deformation points in these regions appear dense when monitoring the deformation. (Figure 7).

Figure 7. Strain analysis of the object points on the dam, ellipse and circle are explained in text.

6. Discussion and conclusion

In this study, to monitor the rate variation of the deformation, we used two methods (terrestrial and GNSS) to obtain the data as given in detail in Section 3. The dam is more stable with respect to about 20 years of terrestrial measurement results (Figure 8).

The determination of the strain field through the downstream and upstream surfaces should contribute to the security of a dam. Different results for the magnitude of the strain values on various

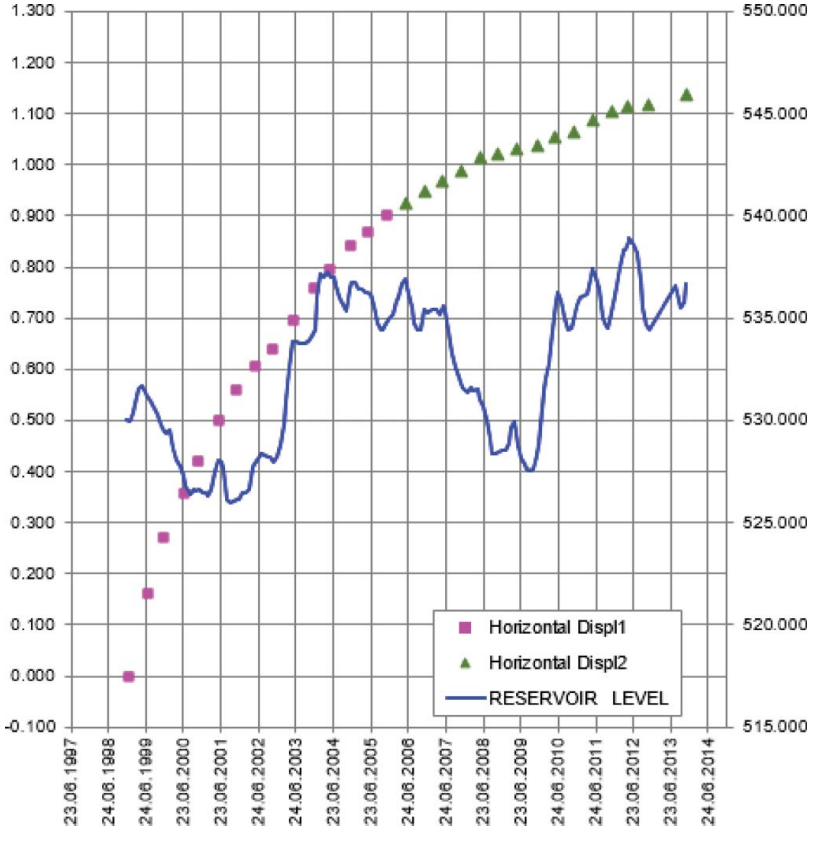

Figure 8. Reservoir water height and horizontal displacements obtained from deformation analysis, squares are horizontal displacement 1 calculated from terrestrial data 1998–2005 (DSI 2005), triangles represent horizontal displacement 2 obtained from terrestrial data 2006–2013.

surfaces can be examined. Correlation between calculated strain fields obtained with different techniques can be analyzed to find out necessary precautions.

In this study, a total of 11 epochs of deformation observations using the terrestrial method and 9 epochs for GNSS methods were carried out between May 2006 and November 2013 under the 'Monitoring the Deformation on Ataturk Dam with Geodetic Method Project.' Data from the field work were evaluated through deformation and strain analysis, and the results are:

According to the strain analysis, the biggest deformation was on the old stream bed. These results are compatible with the results of deformation analysis. According to the strain analysis results, the water level can reach a maximum retention level of 542 m.

According to the classic deformation analysis results for the 11th observation epoch, which was completed in November 2013, 91% of the object points have experienced significant horizontal movement for the last seven years. These results are also compatible, as with the results for embankment dams in these studies (Manake and Kulkarni 2002; Kalkan 2014; Kalkan et al. 2016).

According to these results, the largest movement was on the mid-section of the dam (Figure 4). On point 2082, which is on this section and has a close altitude with the crest, there is a total of 21.1 cm movement on the upstream-downstream direction between 2006–2013 (2nd period-90 months). The movement on the same point between 1997–2005 (1st period-84 months) is given as 87.2 cm (DSI 2005). The monthly average speed on the point for the first period is 10.4 mm, whereas it is 2.3 mm during the second. Average reservoir elevation was determined as 531.0 and 533.8 m for these periods, respectively, and the second period average was 3 m higher than the first. Despite the increase in water level, the deformation velocity on this object point decreased (Pytharouli and Stiros 2005).

In conclusion, it can be seen that dam embankment is now more stabilized, and the movement significantly decreased despite the water load behind the dam reservoir (Figure 8). Based on this, the reservoir water level can be increased gradually over time and will approach 542 m, the maximum water level of the dam. This is important progress. Thus, a 1 cm increase in the reservoir water level is almost equal to 8 million m^3 of water. Continuing to monitor this dam, which is used for irrigation, potable water, and the generation of energy, using data from different techniques is an essential approach.

Acknowledgments

We would like to give thanks to Turkish General Directorate of State Hydrologic Works and the administrative board and surveying team of the Ataturk Dam. The maps and figures were obtained and prepared from Google Earth in June 2017.

Disclosure statement

No potential conflict of interest was reported by the authors.

ORCID

C .O. Yigit http://orcid.org/0000-0002-1942-7667

References

Baarda W. 1973. S-transformation and criterion matrices, Netherlands Geodetic commission, publications on Geodesy. New Ser. 5(1):124–135.

Behr J, Hudnut K, King N. 1998. Monitoring structural deformation at Pacoima dam, California using continuous GPS. Proceedings of the 11th International Technical Meeting of the Satellite Division of the Institute of Navigation (ION GPS 1998) (Vol. 11); Sept 15–18; Nashville, TN. p. 59–68.

Boulanger RW, Montgomery J. 2016. Nonlinear deformation analyses of an embankment dam on a spatially variable liquefiable deposit. Soil Dyn Earthq Eng. 91:222–233.
Brunner FK. 1979. On the analysis of geodetic networks for the determination of the incremental strain tensor. Surv Rev. 25(192):56–67.
Chen B, Gu C, Bao T, Wu B, Su H. 2016. Failure analysis method of concrete arch dam based on elastic strain energy criterion. Eng Fail Anal. 60:363–373.
Cooper MAR. 1987. Control surveys in civil engineering. New York (NY): Nichols Pub Co.
Deniz R. 1990. Determination of local strain in the Earth's crust from geodetic measurements. J Istanbul Tech Univ. 48(4):15–22.
Doğan U. 2017. Investigation of deformation caused by Izmit earthquake in August 1999 with kinematic model [dissertation]. Istanbul: Yıldız Technical University.
DSI (Turkish General Directorate of State Hydrologic Works). 2005. Ataturk Dam and hydroelectric power plant. Ankara: Zurich-Electrowatt Eng. & Ankara-Dolsar Eng. Technical Rep. 2005.
[FEMA] Federal Emergency Management Agency. 2015. Federal guidelines for dam safety risk management. FEMA P-1025. Washington (DC): US Department of Homeland Security.
Gulal E. 2013. Structural deformations analysis by means of Kalman-filtering. Bol Ciênc Geod. 19(1):98–113.
Hekimoglu S, Erdogan B, Butterworth S. 2010. Increasing the efficacy of the conventional deformation analysis methods: alternative strategy. J Surv Eng. 136(2):53–62.
Hoover WE, Rockville MD. 1984. Algorithms for confidence circles and ellipses. Rockville (MD): US Department of Commerce, National Oceanic and Atmospheric Administration, National Ocean Service.
ICOLD BULLETIN 87. 1992. Improvement of existing dam monitoring, recommendations and case histories. Paris: International Commission on Large Dams.
Jansen RB. 1983. Dams and public safety. Washington (DC): US Government Printing Office; 20402 Stock, (024-003).
Kakkuri J, Chen R. 1992. On horizontal crustal strain in Finland. J Geod. 66(1):12–20.
Kalkan Y. 2014. Geodetic deformation monitoring of Ataturk Dam in Turkey. Arab J Geosci. 7(1):397–405.
Kalkan Y, Alkan RM, Bilgi S. 2010. Deformation monitoring studies at Atatürk dam. Sydney (Australia): FIG Congress 2010. Apr. 11–16; p. 1–14.
Kalkan Y, Potts LV, Bilgi S. 2016. Assessment of vertical deformation of the Atatürk dam using Geodetic observations. J Surv Eng. 142(2):04015011. [14 p.].
Kan ME, Taiebat HA. 2016. Application of advanced bounding surface plasticity model in static and seismic analyses of Zipingpu Dam. Can Geotech J. 53(3):455–471.
Koch KR. 1985. A statistical evaluation method for deformation measurements. General Survey News. 92(3):97–108.
Lambeck K. 1979. Methods and geophysical applications of satellite geodesy. Rep Prog Phys. 42(4):547.
Lambeck K. 1988. Geophysical geodesy: the slow deformations of the earth. Oxford: Clarendon; 710 p.
Li W, Wang C. 2011. GPS in the tailings dam deformation monitoring. Procedia Eng. 26:1648–1657.
Liu SH, Wang LJ, Wang ZJ, Bauer E. 2016. Numerical stress-deformation analysis of cut-off wall in clay-core rockfill dam on thick overburden. Water Sci Eng. 9(3):219–226.
Manake A, Kulkarni MN. 2002. Study of the deformation of Koyna dam using the global positioning system. Surv Rev. 36(285):497–507.
Niemeier W. 1985. Deformations analyse. In: Pelzer H, editor. Geodetic networks in land and engineering surveying II. Stuttgart: Taylor & Francis; 559–623.
Pelzer H. 1971. Zur analyse geodätischer deformationsmessungen. Munich: Deutsche Geodätische Kommission. Rep. No.:C-164.
Pelzer H. 1985. Fundamentals of mathematical statistics and balancing calculation. In: Pelzer, H, editor. Geodetic networks in national and engineering surveying II. Surveying Vol. 13, K.diego.
Pesci A, Teza G. 2006. Strain rate analysis over the central Apennines from GPS velocities: the development of a new free software. Boll. Geodesia Sc. Aff. 56:69–88.
Ponseti M, López-Pujol J. 2006. The Three Gorges Dam Project in China: history and consequences. HMiC: història moderna i contemporània. 4:151–188.
Prescott WH. 1976. An extension of Frank's method for obtaining crustal shear strains from survey data. B Seismol Soc Am. 66(6):1847–1853.
Pytharouli SI, Stiros SC. 2005. Ladon dam (Greece) deformation and reservoir level fluctuations: evidence for a causative relationship from the spectral analysis of a geodetic monitoring record. Eng Struct. 27(3):361–370.
Singh V. 2013. Dam breach modeling technology (Vol. 17). Baton Rouge, LA: Springer Science & Business Media, Louisiana State University.
Taşçi L. 2008. Dam deformation measurements with GPS. Geod Cartogr. 34(4):116–121.
Teza G, Pesci A, Galgaro A. 2008. Grid_strain and grid_strain3: software packages for strain field computation in 2D and 3D environments. Comput Geosci. 34(9):1142–1153.
U.S. Army Corps of Engineers (USACE). 2002. Engineering and design structural deformation surveying (EM 1110-2-1009). Washington (DC): Department of the Army, US Army Corps of Engineers; p. 1–292.

Welsch W, Heunecke O, Kuhlmann H. 2000. Evaluation of geodetic monitoring measurements. Karlsruhe: Herbert Wichman Verlag.

Yigit CO, Alcay S, Ceylan A. 2016. Displacement response of a concrete arch dam to seasonal temperature fluctuations and reservoir level rise during the first filling period: evidence from geodetic data. Geomat Nat Hazards Risk. 7 (4):1489–1505.

Zhu-Jiang SHEN, Gang XU. 1996. Deformation behavior of rock materials under cyclic loading. J Nanjing Hydraulic Res Inst. 2:143–150.